Fluorine grafted Cu7S4-Au heterodimers for multimodal imaging guided photothermal therapy with high penetration depth

Jiabin Cui, Rui Jiang, Chang Guo, Xilin Bai, Suying Xu, and Leyu Wang

J. Am. Chem. Soc., **Just Accepted Manuscript** • DOI: 10.1021/jacs.8b00368 • Publication Date (Web): 20 Apr 2018

Fluorine grafted Cu_7S_4-Au heterodimers for multimodal imaging guided photothermal therapy with high penetration depth

Jiabin Cui, Rui Jiang, Chang Guo, Xilin Bai Suying Xu, and Leyu Wang*

State Key Laboratory of Chemical Resource Engineering, Beijing Advanced Innovation Center for Soft Matter Science and Engineering, Beijing University of Chemical Technology, Beijing 100029, China

Supporting Information Placeholder

ABSTRACT: We report the multifunctional nanocomposites (NCs) consisting of ^{19}F-moieties grafted Cu_7S_4-Au nanoparticles (NPs) for negligible background ^{19}F-magnetic resonance imaging (^{19}F-MRI) and computed tomography (CT) imaging guided photothermal therapy. The localized surface plasmon resonance (LSPR) peak can be reasonably tuned to the *in vivo* transparent window (800-900 nm) by coupling Au (<10 nm, LSPR ~530 nm) with Cu_7S_4 (<15 nm, LSPR ~1500 nm) into Cu_7S_4-Au heterodimers. The *in vivo* photothermal tests show that Cu_7S_4-Au show deeper light penetration with 808-nm irradiation, better photothermal efficacy and less damage to normal tissues than Cu_7S_4 with 1500-nm irradiation. Moreover, compared to traditional ^{1}H-MRI, the ^{19}F-MRI based on these NCs demonstrates much better sensitivity due to the negligible background. This work offers a promising strategy for multimodal imaging guided photothermal therapy of deep tissue with good efficacy.

Multimodal imaging-guided photothermal therapy (PTT)[1-3] has been extensively considered as a promising and minimally invasive strategy for cancer therapy. One of the essential requirements in the imaging-guided PTT is the high penetration depth of irradiation and imaging. Due to the high content of water in live body (50-80% in weight),[4, 5] the major challenge to increase the penetration depth is designing the nanoprobes which can effectively dodge the influence of water. In recent years, plasmonic nanostructures including gold nanorods,[6-8] nanocages,[9-11] hollow spheres,[12, 13] and core/shell nanoparticles (NPs)[14-16] with localized surface plasmon resonance (LSPR) peak in the transparent window (800-900 nm)[17, 18] have been recognized as promising agents for PTT.[1, 2, 19] Despite of great progresses,[20-24] it is still urgent to get the strong LSPR absorption in the transparent window, high photothermal conversion efficiency and long-time stability.

In addition to noble metal nanostructures,[25] chalcogenide[26, 27] and metal-oxide[28] nanocrystals also exhibit LSPR features in near infrared (NIR) and mid-infrared (MIR) regions *via* doping, the process of introducing foreign atoms or impurities into a host lattice.[29, 30] In contrast to LSPR in metals, which is attributed to oscillation of free electrons, the LSPR in doped semiconductors arises from free holes as a result of cation vacancies.[31] The hole-density and thus LSPR peak can be readily tuned by varying the doping level.[32, 33] Among these nanocrystals, self-doped copper chalcogenide has been harnessed for many new applications including photocatalysis,[22, 34] photothermal imaging,[35] photo-controlled drug delivery,[36] and PTT,[37-39] however, it is hard to tune the LSPR peak of $Cu_{2-x}S$ to transparent window.[40] The formation of heterodimer has been confirmed as a novel strategy to tune the LSPR peak position.[28, 36, 41-43] Sun[44, 45] has successfully fabricated the Au-Ag heterodimers *via* growing Ag domain on Au seeds. The absorption was enhanced, broadened and red-shifted to 650 nm. By growing $Cu_{2-x}Se$ on Au seeds, Swihart[26] synthesized Au-$Cu_{2-x}Se$ heterodimers with broadened absorption centered at 1120 nm. By means of Au seeds, Jiang[46] synthesized Au-Cu_9S_5 hybrids with LSPR peak at 1100 nm. So far, it remains largely unexplored to get the expected LSPR around 800 nm by growing small Au domain on $Cu_{2-x}S$ NPs.

In another aspect, magnetic resonance imaging (MRI) is one of the most popular imaging techniques,[47, 48] which can be used for imaging deep tissues with negligible injury. However, the conventional ^{1}H MRI suffers from low signal-to-noise ratio (SNR) due to the high content of water in body.[4] Recently, fluorine-19 (^{19}F) MRI with a higher SNR has drawn wide attention, because ^{19}F displays almost equivalent sensitivity to that of ^{1}H (0.83 relative to ^{1}H) and owns negligible endogenous background interference, which complements the wealth of information provided by conventional ^{1}H MRI.[49-51] The major challenge of ^{19}F MRI is to increase the number of ^{19}F atoms per probe and simultaneously retain the molecular mobility, otherwise the ^{19}F MRI signal will be attenuated by the reduced solubility of probes with increased restriction of ^{19}F molecular mobility while grafting more ^{19}F-atom onto one particle.[38, 52, 53] Compared to MRI, computed tomography (CT) is sensitive with a high spatial resolution,[54-56] but is limited by the associated radiation burden and lack of tissue characterization.[57] Simultaneous CT-MRI has potentials to address individual limitations of each imaging modality and enable synergistic physiological and morphologic imaging. Therefore, the CT/^{19}F-MRI guided PTT will be highly desirable imaging-guided ablation strategy but faces challegening.

Herein, we report a facile strategy to get the strong LSPR absorption around ~808 nm by growing a small Au domain (7.3 ± 1.5 nm, LSPR at ~530 nm) on a heavily doped Cu_7S_4 domain (14 ± 0.8 nm, LSPR at ~1500 nm) to form a Cu_7S_4-Au heterodimer (detailed synthesis procedures presented in Supporting Information and Table S1). Then, the ^{19}F-MRI singal molcules were grafted onto the heterodimer *via* click chemistry (Figure S1) to form Cu_7S_4-Au@PSI-^{19}F/PEG nanocomposites (termed as NCs) (Scheme 1). These NCs were successfully utilized for

simultaneous CT/^{19}F-MR imaging guided PTT with negligible background and high penetration depth.

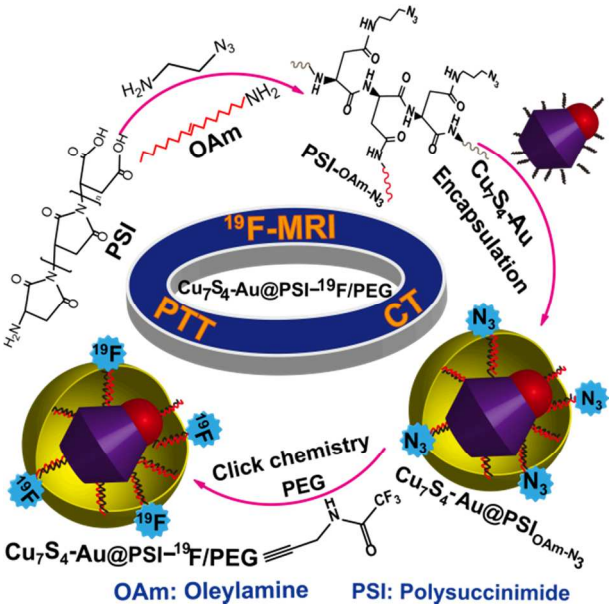

Scheme 1. Schematic illustration for the fabrication and CT/^{19}F-MR imaging guided PTT of Cu_7S_4-Au@PSI-^{19}F/PEG.

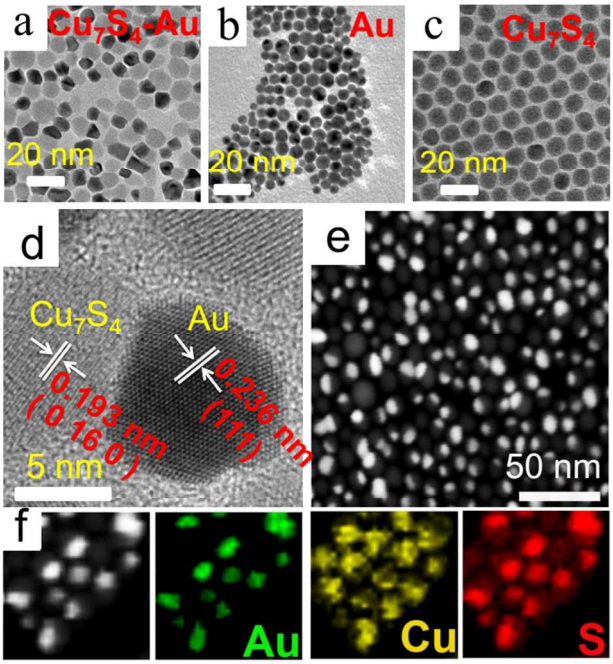

Figure 1. TEM images of Cu_7S_4-Au (**a**), Au (**b**) and Cu_7S_4 (**c**) NPs. HRTEM (**d**), STEM (**e**) images and (**f**) HAADF-STEM image as well as corresponding elemental maps of Cu_7S_4-Au.

Figure 1a shows the typical transmission electron microscope (TEM) image of Cu_7S_4-Au heterodimers obtained by depositing Au (7.3 ± 1.5 nm, Figure 1b) on Cu_7S_4 (14 ± 0.8 nm, Figure 1c).[22] To further confirm the heterostructure, both high resolution transmission electron microscopy (HRTEM) and high-angle annular dark-field scanning transmission electron microscopy (HAADF-STEM) analyses have been carried out. As shown in Figure 1d, the inhomogeneous contrast within each nanoparticle shown on the HRTEM image indicates the heterostructure. HRTEM image also reveals the intimate metal-semiconductor interface and high crystallinity of Cu_7S_4-Au. The lattice fringes with a measured interplanar spacing of 0.193 nm in the semiconductor domain, correspond to the (0 16 0) planes of the Cu_7S_4.[22] In metal domain, an interplanar distance of 0.236 nm is consistent with the (111) lattice spacing of face-centered cubic (fcc) Au. The HAADF-STEM micrograph (Figure 1e) clearly shows that Cu_7S_4-Au NPs are heterodimers (the brighter contrast demonstrates Au) instead of Cu_7S_4@Au core/shell nanostructures. The energy-dispersive spectroscopy (EDS) elemental maps shown in Figure 1f and X-ray photoelectron spectroscopy (XPS) analysis (Figure S2) further confirm the composition of heterodimers. The heterostructure of Cu_7S_4-Au was further confirmed by the powder X-ray diffraction (XRD) patterns in Figure S3.

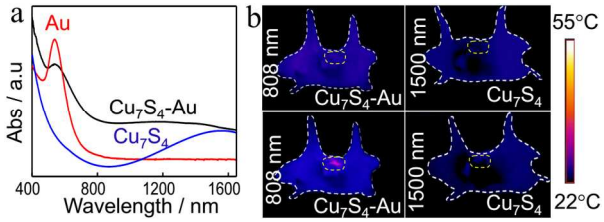

Figure 2. (**a**) LSPR absorption spectra of these NPs. (**b**) Photothermal images of mouse liver injected with Cu_7S_4-Au (left) and Cu_7S_4 (right) NPs before (Top) and after (bottom) irradiation with 808-nm (left) and 1500-nm (right) light after passing through 1.7-cm-thick tissue (initial irradiation: 0.5 W/cm^2; 5 min).

As shown in Figure 2a, after the formation of Cu_7S_4-Au, the visible absorption of Au (LSPR at ~530 nm) slightly weakened and the NIR absorption of Cu_7S_4 (LSPR ~1500 nm) showed slight enhancement. Interestingly, in the NIR region of 700-1500 nm, the LSPR absorption was greatly enhanced, which was as strong as that at 1500 nm. It is noteworthy that, for the LSPR spectrum test, the concentration of Au and Cu_7S_4 in solution was kept identical to that in Cu_7S_4-Au colloids, respectively. We also checked the influence of Au size on the LSPR of Cu_7S_4-Au. As shown in Figure S4, if the Au size was 3.1 ± 0.5 nm, no obvious changes of absorption around 800 nm was observed. When the size was increased to 9.8 ± 1.2 nm, a broad and increased absorption was obtained (Figure S5) as that of Cu_7S_4-Au with Au size of 7.3 ± 1.5 nm. As a control, we could not observe any new absorption enhancement around 800 nm from the physical mixture (Figure S6) of Au (7.3 ± 1.5 nm) and Cu_7S_4 NPs (14 ± 0.8 nm), suggesting that this new absorption around 800 nm arisen from the coupling of these two domains in a heterodimer.

The evolution of LSPR could be mainly attributed to the changes of free carrier concentration, particle size, as well as the refractive index variation of surrounding medium.[31, 32] It is known that the LSPR of Au is attributed to oscillation of free electrons and the LSPR of heavily doped semiconductors (Cu_7S_4) arises from free holes.[58] The formation of Cu_7S_4-Au heterodimers would result in charge neutralization, accordingly red-shift of LSPR for individual domains. Here the enhancement of absorption around 808 nm should be mainly attributed to the red-shift of LSPR of Au domain. With respect to LSPR of Cu_7S_4 domain, the reduction of hole-density results in the simultaneously depressed and broadened absorption spectrum. Meanwhile, given that the refractive index of Cu_7S_4 is higher than that of Au, and thus, the formation of Cu_7S_4-Au heterodimer would lead to red-shift for the LSPR of Au domain and blue-shift for the LSPR of Cu_7S_4 domain. Judging from the experimental observation, the effect of refractive index is dominant for the LSPR change in Cu_7S_4 domain.

As aforementioned, we focus on the ~800 nm region because this special NIR light can effectively dodge the absorption of tissues, blood, and especially water (Figure S7), and thus results

in efficient PTT. In order to understand the influence of irradiation wavelength on the photothermal efficacy, *in vivo* photothermal imaging was conducted. The Cu_7S_4 and Cu_7S_4-Au were injected into liver of the dissected mice first and then the irradiation light passed through 1.7-cm thick tissue from the backside to irradiate the liver with 1500-nm and 808-nm laser, respectively. As shown in Figure 2b, after a 5-min irradiation (0.5 W/cm^2), the photothermal image of liver was clearly observed in the mouse injected with Cu_7S_4-Au under irradiation of 808-nm light, suggesting an obvious photothermal effect. On the contrast, the liver of Cu_7S_4-injected mouse demonstrated no observable temperature increment after exposure to 1500-nm light (0.5 W/cm^2, 5 min), although the absorbance of Cu_7S_4-Au at 808-nm is almost equal to that of Cu_7S_4 at 1500-nm, which is in agreement with the temperature evolution plot (Figure S8). These *in vivo* photothermal imaging results indicate that the 1500-nm is not suitable for deep tissue irradiation due to the serious absorption by water, blood and biological tissues, which was further confirmed by the obvious damage of skin caused by the 1500-nm irradiation (Figure S9).

To explore the bioapplications, the Cu_7S_4-Au NPs were encapsulated with $PSI_{OAm\text{-}N3}$ and then conjugated with 2, 2, 2-trifluoro-N-2-propyn-1-ylacetamide *via* click chemistry (Figure S1). These multifunctional NCs were characterized *via* TEM, dynamic light scattering (DLS), Fourier transform infrared (FTIR) techniques (Figure S10). After ^{19}F-grafting, the particle size (Figure S10) and LSPR absorption (Figure S11) have no obvious change. Both FTIR and ^{19}F-NMR with a single and sharp peak at 75.4 ppm confirmed the ^{19}F grafting (Figure S10). In addition, the tests of pH and temperature influence on ^{19}F-NMR signals of NCs (Figure S12) demonstrate the good stability of NCs. The photothermal efficiency investigation also reveals a satisfied performance of 64.4% for Cu_7S_4-Au NPs at 808-nm irradiation (Figure S13). The cytotoxicity evaluation (Figure S14) confirms the good biocompatibility. Before CT and ^{19}F-MR imaging applications, phantom studies were performed. As shown in Figure S15a, strong CT signals were observed from the colloidal solution, and the CT signal intensity was proportional to the concentration of NCs (C_{NCs}) (Figure S15b). The ^{19}F-MRI was carried out (Figure S16a), and the ^{19}F-MRI signal intensity was proportional to the concentration of fluorine atoms (C_F) (Figure S16b and Figure S17). All the results suggested the great potential of these NCs for both CT and ^{19}F-MR imaging.

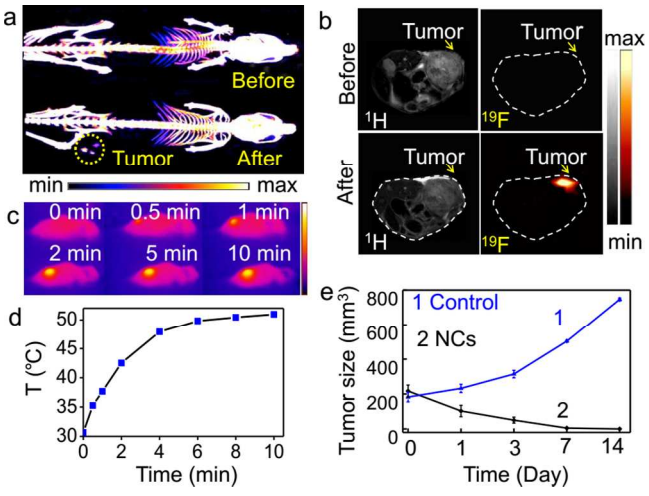

Figure 3. (a) CT images of tumor-bearing mouse before and after the injection of NCs; (b) *In vivo* ^{1}H- and ^{19}F- MRI of the tumor-bearing mice before and after the injection of NCs; (c) photothermal images and (d) temperature evolution profile of the mouse under 808-nm irradiation (1.0 W/cm^2) for 0-10 min; (e) evolution plots of the tumor size after photothermal treatment without (line 1) and with (line 2) NCs injection.

Encouraged by the aforementioned promising results, we carried out the *in vivo* imaging-guided PTT evaluation. As shown in Figure 3a, the tumor with NCs displayed a much bright CT image (HU values before and after injection of NCs were shown in Figure S18). However, in the control mouse without NCs, the tumor was unobservable. In MRI tests, both before and after the injection of NCs, it is hard to clearly delineate the boundary of tumor from surrounding normal tissues in ^{1}H-MRI. As expected, a distinct difference can be observed in ^{19}F-MRI before and after administration of NCs (Figure 3b). Additionally, photothermal properties were examined by irradiation with NIR light (808-nm) at different time intervals. The tumor site displayed a much brighter photothermal image compared with the surroundings (Figure 3c). The temperature at the tumor sites quickly increased from 30 to 51.5 °C within 10 min (Figure 3d), which is highly desirable for PTT. After photothermal treatment, the changes of tumors with initial volume (~200 mm^3) were tracked (Figure S19). As shown in Figure 3e, the tumors completely disappeared after 2 weeks. Meanwhile, the weight of mice increased normally (Figure S20). As a control, if the mouse was treated with light irradiation but without NCs, the tumor grew into a big one after 2 weeks and the weight lost quickly. These observations demonstrate that the Cu_7S_4-Au@PSI-^{19}F/PEG NCs hold potentials as platforms for multimodal imaging-guided PTT with deep penetration.

In summary, we report the multifunctional Cu_7S_4-Au@PSI-^{19}F/PEG for the CT/^{19}F-MR imaging-guided photothermal ablation of tumors with deep penetration. By coupling small Au with Cu_7S_4 NPs, the LSPR peak of the Cu_7S_4-Au heterodimers was reasonably tuned to the *in vivo* transparent window (~800 nm), which greatly enhances the photothermal efficacy and decrease the optical damage to normal tissues. The grafted fluorine moieties render these NCs ^{19}F-MRI ability with negligible background and good sensitivity. Meanwhile, the gold domains enable the NCs CT imaging capability with high spatial resolution. The *in vivo* test results suggest that the CT/^{19}F-MRI multimodal imaging-guided photothermal ablation may become an invaluable tool for fundamental understanding, diagnostics and therapy of tumors. This work paves the way for the rational design of multifunctional nanoplatforms for deep non-invasive imaging-guided photothermal ablation.

ASSOCIATED CONTENT

Supporting Information

Detailed experiments, Table S1, and Figures S1−S20. This material is available free of charge via the Internet at http://pubs.acs.org.

AUTHOR INFORMATION

Corresponding Author

lywang@mail.buct.edu.cn.

Notes

The authors declare no competing financial interests.

ACKNOWLEDGMENT

This research was supported by the National Natural Science Foundation of China (21725501, 21475007, 21675009 and 21505003), and the Fundamental Research Funds for the Central Universities (buctrc201706 and buctrc201720). We thank Prof. X. Zhang at Xiamen University for the help on the ^{19}F MRI and CT

experiments. We also thank the "Public Hatching Platform for Recruited Talents of Beijing University of Chemical Technology".

REFERENCES

(1) Zhang, Z. J.; Wang, J.; Nie, X.; Wen, T.; Ji, Y. L.; Wu, X. C.; Zhao, Y. L.; Chen, C. Y. *J. Am. Chem. Soc.* **2014,** *136*, 7317-7326.

(2) Ye, E. Y.; Win, K. Y.; Tan, H. R.; Lin, M.; Teng, C. P.; Mlayah, A.; Han, M. Y. *J. Am. Chem. Soc.* **2011,** *133*, 8506-8509.

(3) Fan, W. P.; Yung, B.; Huang, P.; Chen, X. Y. *Chem. Rev.* **2017,** *117*, 13566-13638.

(4) Chumlea, W. C.; Guo, S. S.; Zeller, C. M.; Reo, N. V.; Siervogel, R. M. *Kidney Int.* **1999,** *56*, 244-252.

(5) Xiao, Q. F.; Zheng, X. P.; Bu, W. B.; Ge, W. Q.; Zhang, S. J.; Chen, F.; Xing, H. Y.; Ren, Q. G.; Fan, W. P.; Zhao, K. L.; Hua, Y. Q.; Shi, J. L. *J. Am. Chem. Soc.* **2013,** *135*, 13041-13048.

(6) Song, T. J.; Tang, L. H.; Tan, L. H.; Wang, X. J.; Satyavolu, N. S. R.; Xing, H.; Wang, Z. D.; Li, J. H.; Liang, H. J.; Lu, Y. *Angew. Chem.-Int. Edit.* **2015,** *54*, 8114-8118.

(7) Bagley, A. F.; Hill, S.; Rogers, G. S.; Bhatia, S. N. *ACS Nano* **2013,** *7*, 8089-8097.

(8) Jiang, R. B.; Chen, H. J.; Shao, L.; Li, Q.; Wang, J. F. *Adv. Mater.* **2012,** *24*, OP200-OP207.

(9) Camposeo, A.; Persano, L.; Manco, R.; Wang, Y.; Del Carro, P.; Zhang, C.; Li, Z. Y.; Pisignano, D.; Xia, Y. N. *ACS Nano* **2015,** *9*, 10047-10054.

(10) Gao, H.; Liu, R.; Gao, F. P.; Wang, Y. L.; Jiang, X. L.; Gao, X. Y. *ACS Nano* **2014,** *8*, 7260-7271.

(11) Xia, Y. N.; Li, W. Y.; Cobley, C. M.; Chen, J. Y.; Xia, X. H.; Zhang, Q.; Yang, M. X.; Cho, E. C.; Brown, P. K. *Accounts Chem. Res.* **2011,** *44*, 914-924.

(12) Chandra, M.; Dowgiallo, A. M.; Knappenberger, K. L. *J. Am. Chem. Soc.* **2010,** *132*, 15782-15789.

(13) Mahmoud, M. A.; O'Neil, D.; El-Sayed, M. A. *Chem. Mater.* **2014,** *26*, 44-58.

(14) Goodman, A. M.; Cao, Y.; Urban, C.; Neumann, O.; Ayala-Orozco, C.; Knight, M. W.; Joshi, A.; Nordlander, P.; Halas, N. J. *ACS Nano* **2014,** *8*, 3222-3231.

(15) Ma, Y. Y.; Li, W. Y.; Cho, E. C.; Li, Z. Y.; Yu, T. K.; Zeng, J.; Xie, Z. X.; Xia, Y. N. *ACS Nano* **2010,** *4*, 6725-6734.

(16) Bardhan, R.; Lal, S.; Joshi, A.; Halas, N. J. *Accounts Chem. Res.* **2011,** *44*, 936-946.

(17) Weissleder, R. *Nat. Biotechnol.* **2001,** *19*, 316-317.

(18) Hong, G. S.; Robinson, J. T.; Zhang, Y. J.; Diao, S.; Antaris, A. L.; Wang, Q. B.; Dai, H. J. *Angew. Chem.-Int. Edit.* **2012,** *51*, 9818-9821.

(19) Huang, P.; Lin, J.; Li, W. W.; Rong, P. F.; Wang, Z.; Wang, S. J.; Wang, X. P.; Sun, X. L.; Aronova, M.; Niu, G.; Leapman, R. D.; Nie, Z. H.; Chen, X. Y. *Angew. Chem.-Int. Edit.* **2013,** *52*, 13958-13964.

(20) Castellana, E. T.; Gamez, R. C.; Russell, D. H. *J. Am. Chem. Soc.* **2011,** *133*, 4182-4185.

(21) Gao, C. B.; Lu, Z. D.; Liu, Y.; Zhang, Q.; Chi, M. F.; Cheng, Q.; Yin, Y. D. *Angew. Chem.-Int. Edit.* **2012,** *51*, 5629-5633.

(22) Cui, J. B.; Li, Y. J.; Liu, L.; Chen, L.; Xu, J.; Ma, J. W.; Fang, G.; Zhu, E. B.; Wu, H.; Zhao, L. X.; Wang, L. Y.; Huang, Y. *Nano Lett.* **2015,** *15*, 6295-6301.

(23) Hu, Y. X.; Liu, Y. Z.; Li, Z.; Sun, Y. G. *Adv. Funct. Mater.* **2014,** *24*, 2828-2836.

(24) Yang, H.; He, L. Q.; Hu, Y. W.; Lu, X. H.; Li, G. R.; Liu, B. J.; Ren, B.; Tong, Y. X.; Fang, P. P. *Angew. Chem.-Int. Edit.* **2015,** *54*, 11462-11466.

(25) Li, Z.; Foley, J. J.; Peng, S.; Sun, C. J.; Ren, Y.; Wiederrecht, G. P.; Gray, S. K.; Sun, Y. G. *Angew. Chem.-Int. Edit.* **2015,** *54*, 8948-8951.

(26) Liu, X.; Lee, C.; Law, W. C.; Zhu, D. W.; Liu, M. X.; Jeon, M.; Kim, J.; Prasad, P. N.; Kim, C.; Swihart, M. T. *Nano Lett.* **2013,** *13*, 4333-4339.

(27) Costi, R.; Saunders, A. E.; Banin, U. *Angew. Chem.-Int. Edit.* **2010,** *49*, 4878-4897.

(28) Ye, X. C.; Hickey, D. R.; Fei, J. Y.; Diroll, B. T.; Paik, T.; Chen, J.; Murray, C. B. *J. Am. Chem. Soc.* **2014,** *136*, 5106-5115.

(29) Ma, G. X.; Zhou, Y. L.; Li, X. Y.; Sun, K.; Liu, S. Q.; Hu, J. Q.; Kotov, N. A. *ACS Nano* **2013,** *7*, 9010-9018.

(30) Ye, X. C.; Fei, J. Y.; Diroll, B. T.; Paik, T.; Murray, C. B. *J. Am. Chem. Soc.* **2014,** *136*, 11680-11686.

(31) Luther, J. M.; Jain, P. K.; Ewers, T.; Alivisatos, A. P. *Nat. Mater.* **2011,** *10*, 361-366.

(32) Liu, X.; Swihart, M. T. *Chem. Soc. Rev.* **2014,** *43*, 3908-3920.

(33) Hsu, S. W.; Bryks, W.; Tao, A. R. *Chem. Mater.* **2012,** *24*, 3765-3771.

(34) Cui, J.; Jiang, R.; Lu, W.; Xu, S.; Wang, L. *Small* **2017,** *13*, 1602235-1602241.

(35) Cui, J. B.; Xu, S. Y.; Guo, C.; Jiang, R.; James, T. D.; Wang, L. Y. *Anal. Chem.* **2015,** *87*, 11592-11598.

(36) Huang, S.; Liu, J.; He, Q.; Chen, H. L.; Cui, J. B.; Xu, S. Y.; Zhao, Y. L.; Chen, C. Y.; Wang, L. Y. *Nano Res.* **2015,** *8*, 4038–4047.

(37) Liu, X.; Wang, X. L.; Swihart, M. T. *Chem. Mater.* **2013,** *25*, 4402-4408.

(38) Hu, G. F.; Li, N. N.; Tang, J.; Xu, S.; Wang, L. Y. *ACS Appl. Mater. Interfaces* **2016,** *8*, 22830–22838.

(39) Hu, G. F.; Tang, J.; Bai, X. L.; Xu, S. Y.; Wang, L. Y. *Nano Res.* **2016,** *9*, 1630-1638.

(40) Tian, Q. W.; Tang, M. H.; Sun, Y. G.; Zou, R. J.; Chen, Z. G.; Zhu, M. F.; Yang, S. P.; Wang, J. L.; Wang, J. H.; Hu, J. Q. *Adv. Mater.* **2011,** *23*, 3542-3547.

(41) Jiang, R. B.; Li, B. X.; Fang, C. H.; Wang, J. F. *Adv. Mater.* **2014,** *26*, 5274-5309.

(42) Shaviv, E.; Schubert, O.; Alves-Santos, M.; Goldoni, G.; Di Felice, R.; Vallee, F.; Del Fatti, N.; Banin, U.; Sonnichsen, C. *ACS Nano* **2011,** *5*, 4712-4719.

(43) Banin, U.; Ben-Shahar, Y.; Vinokurov, K. *Chem. Mater.* **2014,** *26*, 97-110.

(44) Sun, Y. G.; Foley, J. J.; Peng, S.; Li, Z.; Gray, S. K. *Nano Lett.* **2013,** *13*, 3958-3964.

(45) Sun, Y. G. *Natl. Sci. Rev.* **2015,** *2*, 329-348.

(46) Ding, X. G.; Liow, C. H.; Zhang, M. X.; Huang, R. J.; Li, C. Y.; Shen, H.; Liu, M. Y.; Zou, Y.; Gao, N.; Zhang, Z. J.; Li, Y. G.; Wang, Q. B.; Li, S. Z.; Jiang, J. *J. Am. Chem. Soc.* **2014,** *136*, 15684-15693.

(47) Dong, L.; Qian, J. C.; Hai, Z. J.; Xu, J. Y.; Du, W.; Zhong, K.; Liang, G. L. *Anal. Chem.* **2017,** *89*, 6922-6925.

(48) Yuan, Y.; Ge, S. C.; Sun, H. B.; Dong, X. J.; Zhao, H. X.; An, L. N.; Zhang, J.; Wang, J. F.; Hu, B.; Liang, G. L. *ACS Nano* **2015,** *9*, 5117-5124.

(49) George, C.; Chandrakumar, N. *Angew. Chem., Int. Ed.* **2014,** *53*, 8441-8444.

(50) Tirotta, I.; Dichiarante, V.; Pigliacelli, C.; Cavallo, G.; Terraneo, G.; Bombelli, F. B.; Metrangolo, P.; Resnati, G. *Chem. Rev.* **2015,** *115*, 1106-1129.

(51) Yamaguchi, K.; Ueki, R.; Nonaka, H.; Sugihara, F.; Matsuda, T.; Sando, S. *J. Am. Chem. Soc.* **2011,** *133*, 14208-14211.

(52) Chen, H. L.; Song, M. L.; Tang, J.; Hu, G. F.; Xu, S. Y.; Guo, Z. D.; Li, N. N.; Cui, J. B.; Zhang, X. Z.; Chen, X. Y.; Wang, L. Y. *ACS Nano* **2016,** *10*, 1355-1362.

(53) Guo, C.; Xu, M. M.; Xu, S. Y.; Wang, L. Y. *Nanoscale* **2017,** *9*, 7163-7168.

(54) Liu, Y. L.; Ai, K. L.; Liu, J. H.; Yuan, Q. H.; He, Y. Y.; Lu, L. H. *Angew. Chem.-Int. Edit.* **2012,** *51*, 1437-1442.

(55) Lu, X. Q.; Li, Y. B.; Bai, X. L.; Hu, G. F.; Wang, L. Y. *Sci. China-Mater.* **2017,** *60*, 777-788.

(56) Chou, S. W.; Shau, Y. H.; Wu, P. C.; Yang, Y. S.; Shieh, D. B.; Chen, C. C. *J. Am. Chem. Soc.* **2010,** *132*, 13270-13278.

(57) Wang, G.; Kalra, M.; Murugan, V.; Xi, Y.; Gjesteby, L.; Getzin, M.; Yang, Q. S.; Cong, W. X.; Vannier, M. *Med. Phys.* **2015,** *42*, 5879-5889.

(58) Comin, A.; Manna, L. *Chem. Soc. Rev.* **2014,** *43*, 3957-3975.

Table of Contents

Multifunctional Cu_7S_4-Au@PSI-^{19}F/PEG nanoprobes are reported for CT/^{19}F-MR dual-modal imaging-guided photothermal ablation with high penetration depth and negligible background.